molecular pharmaceutics



Article

# PET Imaging of VCAM-1 Expression and Monitoring Therapy Response in Tumor with a 68Ga-labeled Single Chain Variable Fragment

Xiao Zhang, Chunbao Liu, Fan Hu, Yingying Zhang, Jing Wang, Yongheng Gao, Yaqun Jiang, Yongxue Zhang, and Xiaoli Lan

*Mol. Pharmaceutics*, **Just Accepted Manuscript** • DOI: 10.1021/acs.molpharmaceut.7b00961 • Publication Date (Web): 08 Jan 2018





ACS Publications

Molecular Pharmaceutics is published by the American Chemical Society. 1155 Sixteenth Street N.W., Washington, DC 20036

# PET Imaging of VCAM-1 Expression and Monitoring Therapy Response in Tumor with a $^{68}$Ga-labeled Single Chain Variable Fragment

**Running title:** Imaging VCAM-1 with PET

Xiao Zhang,[†,‡] Chunbao Liu,[†,‡] Fan Hu,[†,‡] Yingying Zhang,[†,‡] Jing Wang,[§] Yongheng Gao,[§] Yaqun Jiang,[†,‡] Yongxue Zhang,*[,†,‡] Xiaoli Lan*[,†,‡]

[†] Department of Nuclear Medicine, Union Hospital, Tongji Medical College, Huazhong University of Science and Technology, Wuhan 430022, China

[‡] Hubei Key Laboratory of Molecular Imaging, Union Hospital, Tongji Medical College, Huazhong University of Science and Technology, Wuhan 430022, China

[§] Department of Nuclear Medicine, Xijing Hospital, Fourth Military Medical University, Xi'an, 710032, China

**Corresponding Authors**

*Lan X: Department of Nuclear Medicine, Union Hospital, Tongji Medical College, Huazhong University of Science and Technology. Address: No. 1277 Jiefang Ave, Wuhan, Hubei Province 430022, China. Tel: +86-27-83692633, +86-13886193262(mobile). Fax: +86-27-85726282. E-mail: LXL730724@ hotmail.com.

*Zhang Y: Department of Nuclear Medicine, Union Hospital, Tongji Medical College, Huazhong University of Science and Technology. Address: No. 1277 Jiefang Ave, Wuhan, Hubei Province 430022, China. Tel: +86-27-85726282, +86-13807104287 (mobile). Fax: +86-27-85726282. E-mail: zhyx1229@163.com.

**Funding:**

This work was supported by the National Natural Science Foundation of China (No. 81271623 and 81630049), and Clinical Research Physician Program of Tongji Medical College, Huazhong University of Science and Technology (5001530008).

**Disclosure:**

The authors declare no potential conflicts of interest.

**ABSTRACT GRAPHIC**

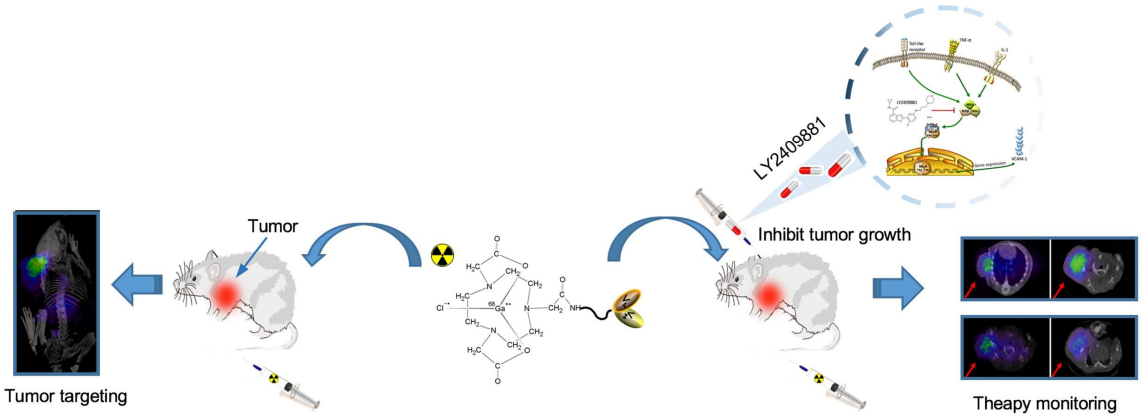

**Abstract**

Vascular cell adhesion molecule-1 (VCAM-1) is a transmembrane glycoprotein closely related to tumorigenicity as well as tumor metastasis. It is also a well-known candidate for detecting tumors. LY2409881, an IKKβ inhibitor, could induce apoptosis of VCAM-1 positive cells. Our purpose is to prepare a novel tracer to evaluate its feasibility of detecting VCAM-1 expression and monitoring LY2409881 tumor curative effect. The tracer was composed of conjugating the single chain variable fragment (scFv) of VCAM-1 and NOTA-NHS-ester, then labeled with $^{68}$Ga. $^{68}$Ga-NOTA-VCAM-1$_{scFv}$ was successfully prepared with high radiochemical yield. VCAM-1 overexpression and underexpression melanoma cell lines, B16F10 and A375m, were used in this study. The results of microPET/CT imaging in small animals indicated that the uptake of $^{68}$Ga-NOTA-VCAM-1$_{scFv}$ in B16F10 tumor was much higher than that of A375m, which was also confirmed by the biodistribution and autoradiography results. LY2409881 inhibits the growth of B16F10 melanoma *in vivo* by inducing dose- and time-dependent growth inhibition and apoptosis of the cells. The LY2409881 treated group and DMSO control group were established and imaged by microPET/CT. In LY2409881 group, uptake of the tracer in tumor was decreased at the first week, and then gradually recovered to the initial level. In DMSO control, the uptake of the tracer kept at the same level during the whole time. The results suggested that LY2409881 inhibits the expression of VCAM-1 and suppresses tumor growth. $^{68}$Ga-NOTA-VCAM-1$_{scFv}$, an easily synthesized probe, has a potential clinical application in the visual monitoring of IKKβ inhibitor intervention on VCAM-1 positive tumors.

**Keywords:** Vascular Cell Adhesion Molecule-1; Single Chain Variable Fragment; $^{68}$Ga; Positron-Emission Tomography; Therapy monitoring

## INTRODUCTION

Vascular cell adhesion molecule 1 (VCAM-1) encodes a cell surface sialoglycoprotein,[1] which is hallmarked by a growing insight into various functionalities in tumorigenicity and metastasis currently.[2] Inhibition of VCAM-1 may effectively regulate cancer cell biological activity and tumor growth.[3] The VCAM-1 expression is correlated with grim outcome and early recurrence in several tumors,[4,5] and down-regulation of VCAM-1 expression has shed light on oncologic therapy.[6,7]

Activation of NF-κB could increase the expression of downstream signaling molecules like VCAM-1 (Figure 1), then promote cell proliferation and tumor growth.[4,8] Currently, LY2409881, a novel, potent and specific IκB kinase β (IKKβ/IKK2) inhibitor, has been identified to present the cytotoxicity to SKOV3 and lymphoma cell lines via inhibition of NF-κB signaling pathway activation.[9] However, the influence of LY2409881 on expressing VCAM-1 and biological function in VCAM-1 positive tumors has not yet been reported.

Precision medicine has become a valuable methodology, and refined disease classification is essential to targeted treatment. It may be helpful to identify VCAM-1 overexpression in patients for individualized treatment options. Compared with common applied immunohistochemical analysis,[10] molecular imaging is a noninvasive quantitative examination that may be useful to determine the expression level of VCAM-1. Some studies have reported imaging of VCAM-1, such as monoclonal antibodies conjugated to microbubbles or iron oxide particles.[11,12] To overcome the slow clearance and poor tissue penetration of intact monoclonal antibodies,[13] small antibody fragments and peptides bound to VCAM-1, including single chain variable fragment (scFv) labeled by $^{99m}$Tc,[13] nanobodies coupled with $^{18}$F or $^{99m}$Tc,[14,15] and peptides labeled by $^{18}$F or $^{99m}$Tc,[16,17] have shown improved image quality. Most of the above-mentioned probes were applied in atherosclerosis. Recently, VCAM-1-$^{111}$In peptide, a SPECT tracer, was used to monitor platinum-based chemotherapy efficacy in metastatic ovarian cancer, and displayed potential to improve management of the disease.[18]

This study has three main aims. First, with the aim of using molecular imaging to identify VCAM-1 expression and its changes with therapy, we developed a molecular probe, $^{68}$Ga-NOTA-VCAM-1$_{scFv}$, in which NOTA-NHS-ester was employed as a sequestrant to trap $^{68}$Ga to VCAM-1 scFv. We evaluated its targeting ability to VCAM-1. Second, we want to evaluate therapeutic activity of LY2409881 on VCAM-1 positive cells and tumors. Last, we want to monitor the therapeutic effect with $^{68}$Ga-NOTA-VCAM-1$_{scFv}$ targeting for VCAM-1. The mechanism of monitoring VCAM-1 changes after LY2309881 therapy by $^{68}$Ga-NOTA-VCAM-1$_{scFv}$ was shown in Figure 1. The final objective was to explore the feasibility of $^{68}$Ga-NOTA-VCAM-1$_{scFv}$, a PET tracer, in detecting the expression of VCAM-1 in tumor and monitoring LY2409881 tumor curative effect.

## MATERIALS AND METHODS

**Reagents and Instruments.** All chemicals were obtained from Sigma Aldrich ( Louis, MO, USA ) . $^{68}$Ga was produced from a $^{68}$Ge/$^{68}$Ga generator (Isotope Technologies Garching GmbH, Garching, Germany) by standard procedures. The scFv of VCAM-1 (Shanghai Raygene Biotech Company, Shanghai, China, http://raygene.bioon.com.cn) was performed by the phage display method as previously described.[19] The NOTA-NHS-ester was obtained from Macrocyclis (Dallax, TX, USA). The different sample radioactivities were counted with automatic well-type gamma counter (PerkinElmer WIZARD2 2470, USA). The imaging experiments were performed on microPET/CT (Mediso, Budapest, Hungary). LY2409881 (IKK2 inhibitor) and temozolomide were from Selleck Chemicals (Houston, TX, USA) and kept in dimethyl sulfoxide (DMSO) at -80 °C. CCK8 was purchased from SAB (College Park, Maryland, USA).

**Radiolabeled probe preparation and identification.** NOTA-NHS, 100 nmol, was added to the scFv of VCAM-1 (28 nmol), and reacted in darkness overnight at 4°C. $^{68}GaCl_3$ was obtained from the $^{68}$Ge/$^{68}$Ga generator by elution with 0.05 M HCl and sodium acetate (1.25 M, pH=8.6) was used to adjust the pH to 3.7. After purification (Zeba Spin Desalting Column, Thermo Fisher Scientific, Fairlawn NJ, USA), 800 μL $^{68}GaCl_3$ (296–370 MBq) was added to the reaction, and maintained for 30 min to prepare $^{68}$Ga-NOTA-VCAM-$1_{scFv}$. The radiochemical yield, radiochemical purity, and *in vitro* stability of the probe (0.5, 1, and 3 h in human serum) were measured by ITLC using 50% acetonitrile and 0.01 M PBS as the developing solvent system.

**Cell culture and identification.** All experiments with the melanoma cell lines, B16F10 and A375m, were carried out within 6 months of receipt or resuscitation after cryopreservation. The Short Tandem Repeat (STR) profiling was used to test and authenticate the cell lines. All cell lines were cultivated in DMEM (Gibco, Grand Island, NY, US) and the VCAM-1 expression levels of B16F10 and A375m cells were confirmed by immunofluorescence study and western blot. Detail methods were described in the Supplementary Materials.

**MicroPET/CT imaging.** The mouse experiments were reviewed and approved by the Animal Care Committee of Tongji Medical College, Huazhong University of Science and Technology. All mice were obtained from Beijing HFK Bioscience Co. Ltd (Beijing, China). B16F10 cells ($1 \times 10^5$) and A375m cells ($5 \times 10^6$) were subcutaneously injected into C57BL/6 mice and BALB/C nude mice in 150 μL PBS per injection in the front flank, respectively. Three weeks after B16F10 and A375m cell injections, the mice were prepared for microPET/CT study.

All mice received intraperitoneal anesthesia with a mixture of ketamine/xylazine (110/10 μg/g) and $^{68}$Ga-NOTA-VCAM-$1_{scFv}$ (500–800 μCi/150 μL) was injected into mice via the tail vein. All B16F10 mice

were imaged at 0.5, 1 and 3 h post-injection. A375m mice were scanned at 3 h as a control group. After imaging, the tumors were removed to check the expression of VCAM-1 with immunohistochemistry (IHC). The detail methods were described in the Supplementary Materials.

**Autoradiography.** The mice bearing B16F10 and A375m xenograft tumors were sacrificed after imaging. The tumor, liver and kidneys were immediately dissected and sliced for autoradiography (ARG). Tissue slices were exposed on the phosphor screen for 120 min, followed by scanning in the Storage Phosphor Imaging System (PerkinElmer Cyclone Plus, USA) to acquire ARG images.

**Biodistribution study.** At 0.5, 1, and 3 h after $^{68}$Ga-NOTA-VCAM-1$_{scFv}$ injection, the A375m (*n*=5 per group) and B16F10 (*n*=5 per group) mice were euthanatized, and the interested samples were collected, weighed and counted with an automatic gamma counter. The radioactivity in organs and tissues were calculated as the percentage of injected dose per gram of tissue (% ID/g) and corrected for radioactive decay.

***In vitro* VCAM-1 inhibition assays with LY2409881 and cell viability.** Quantities of $2\times10^6$/well and $2\times10^5$/well of B16F10 cells were planted into 6-well and 24-well plates, respectively, followed by addition of increasing concentrations (0–20 μM) of LY2409881, and then incubated for 12 h. The VCAM-1 expression levels were detected by western blot in 6-well plates. The cell uptake of the probe was measured in the 24-well plates. Briefly, the cells were incubated with $^{68}$Ga-NOTA-VCAM-1$_{scFv}$ (500 μL, 2 nM in DMEM without serum) for 120 min. Thereafter, the cells were rinsed twice with 1 mL PBS and lysed with 1 M NaOH. The radioactivity in the cell lysate was determined on an automatic gamma counter.

Cell viability after LY2409881 and temozolomide (diluent-specific control) treatment was evaluated by CCK8 assay. A total of $6\times10^3$ B16F10 cells were planted into 96-well plates and kept in cell incubator overnight, then increasing concentrations of LY2409881 (1–40 μM), or temozolomide (100–800 μM) was added and cultured for 24, 48, and 72 h. The one-half maximal inhibitory concentration ($IC_{50}$) was calculated using GraphPad Prism (La Jolla CA, USA).

**Tumor xenografts and *in vivo* LY2409881 treatment.** To evaluate the therapeutic efficacy of LY2409881, a cohort of male C57BL/6 mice (*n*=70) was injected with B16F10 cells. When the B16F10 tumors achieved a size of 50 mm$^3$, the mice were randomly divided into two groups: (a) LY2409881 (100 mg/kg body weight, *n*=35), (b) control group, which received the equal volume of DMSO (diluent-specific control, *n*=35). LY2409881 and control were administered intraperitoneally twice a week. The effect of drug treatment was observed via the tumor size and weight of the mice (*n*=10 each group) until the death of the mice. Tumor volume was determined by width$^2$×length×0.52. The LY2409881 treated mice and the DMSO controls were imaged by microPET/CT (*n*=5 per group) subsequently at 0, 1, 2, and 3 weeks after

initiation of therapy, and the biodistribution of $^{68}$Ga-NOTA-VCAM-1$_{scFv}$ in tumors of the two groups at different weeks (*n*=5 per group) were assessed. MicroPET/CT images were applied to study the growth of tumor. The mice were sacrificed after imaging and blood test, H&E staining of the liver, kidneys, and spleen was performed. Figure 2 shows the flow chart of the treatment groups.

**Statistical analysis.** The data are described as mean ± SD. Statistical analysis was analyzed by Student's *t*-test (two-tailed) or ANOVA, using GraphPad Prism, and $p<0.05$ was considered significant. The Kaplan–Meier time-to-sacrifice analysis was used to calculate the estimated survival distribution in the therapeutic study.

## RESULTS

**VCAM-1 expression in B16F10 and A375m cells.** Immunofluorescence staining experiments were carried out in B16F10 and A375m cells to determine VCAM-1 expression levels. A strong fluorescence intensity was observed in B16F10 cells, but the A375m cells were weakly positive (Figure 3A). The results of western blot and the integrated optical density analysis again show much more VCAM-1 expressed in B16F10 cells. (Figure 3B and 3C).

**Targeting ability of $^{68}$Ga-NOTA-VCAM-1$_{scFv}$ to VCAM-1 and its biodistribution.** The radiochemical yield of $^{68}$Ga-NOTA-VCAM-1$_{scFv}$ was 96.92 ± 2.02% with specific activity of 10.17 ± 1.01 MBq/nmol and radiochemical purity of 96.97 ± 2.13% (*n*=6). The radiochemical purities of $^{68}$Ga-NOTA-VCAM-1$_{scFv}$ maintained > 90% at 0.5, 1, and 3 h in human serum, indicating the tracer had a high stability *in vitro* (Supplemental Materials Figure S1).

The microPET/CT images of B16F10 and A375m xenograft tumors are shown in Figure 4A and 4B. The uptake of $^{68}$Ga-NOTA-VCAM-1$_{scFv}$ in B16F10 tumor was visualized clearly at different scan time points. In contrast, the tracer accumulation in A375m tumor was very low. These results confirm that $^{68}$Ga-NOTA-VCAM-1$_{scFv}$ can bind to VCAM-1 positive tumors *in vivo* and demonstrates good tumor retention.

Besides, blood pool activity was visualized in the heart at 0.5 h. The distribution of $^{68}$Ga-NOTA-VCAM-1$_{scFv}$ in blood was 5.96 ± 0.35 and 2.52 ± 0.18% ID/g at 0.5 and 3 h post-injection, which demonstrated a relatively rapid clearance in blood. The uptake in the kidneys was high, which suggested for renal excretion as the main clearance pathway. Liver uptake was noticed first at 60 min, and then decreased sharply. The ARG and IHC study also showed different levels of VCAM-1 expression in B16F10 (high) and A375m (low) tumor tissues (Figure 4C-4E).

The biodistribution results are shown in Figure 5. The radioactivities in kidneys were the highest in both models (Figure 5A and 5B), which was same with the imaging, again suggesting that renal clearance is the primary removal pathway of $^{68}$Ga-NOTA-VCAM-1$_{scFv.}$ The tumor uptakes in B16F10 mice were much higher than those of A375m (Figure 5C) at different time points post-injection. Significantly higher tumor-to-muscle ratios (T/M) (Figure 5D) and tumor-to-blood ratios (T/B) (Figure 5E) were recorded in B16F10 models than in A375m models.

**LY2409881 effect on cell growth, VCAM-1 expression and cellular uptake of $^{68}$Ga-NOTA-VCAM-1$_{scFv}$ *in vitro.*** After LY2409881 treatment for 12 h, western blot showed decreased expression of VCAM-1 in B16F10 cells (Figure 6A and 6B). The uptake of $^{68}$Ga-NOTA-VCAM-1$_{scFv}$ declined dramatically when exposed to only 2 μM LY2409881, reaching a plateau at concentrations > 2 μM (Figure 6C). These results indicate that LY2409881 inhibits the expression of VCAM-1 resulting in decreased binding of $^{68}$Ga-NOTA-VCAM-1$_{scFv}$ to B16F10 cells in a dose-dependent manner. The binding affinities and specificities of $^{68}$Ga-NOTA-VCAM-1$_{scFv}$ with VCAM-1 were verified with LY2409881 as an inhibition reagent. Cell viability after LY2409881 and temozolomide (an antitumor drug) treatment for 24, 48, and 72 h is shown in Figure 6D and 6E. After drug treatment, B16F10 cells showed a concentration- and time-dependent increase in apoptosis. Compared to 565.90 μM for temozolomide, the $IC_{50}$ values of LY2409881 in B16F10 cells was 17.69 μM at 24 h, which implies that LY2409881 was a stronger growth inhibitor.

**LY2409881 inhibits tumor growth and its influence on the animal models.** The growth of B16F10 xenograft tumors was assessed to identify the potential activity of LY2409881 *in vivo*. In contrast with the control group, LY2409881 treatment significantly reduced the tumor size (Figure 7A). Meanwhile, the growth velocity of the treatment and control group was 58.30 ± 8.51 and 123.70 ± 20.99 mm$^3$/d ($n$=10 per group, $p < 0.01$), respectively, and the tumor inhibitory ratio on day 21 was 51.76%. The model weight of the two groups had no statistical difference (Figure 7B). The death of all mice marked the end of the observation. The median survival time for the treatment group and control group were 29.9 d and 25.0 d, respectively (Figure 7C, $p < 0.001$). These results demonstrated that LY2409881 effectively inhibited B16F10 tumor growth. Organs or tissues, such as blood, livers, kidneys and spleens, were also evaluated for functional or pathological changes. The results showed that there was no obvious damage to these organs with LY2409881 treatment (Table 1, Figure 7D). The above results indicate that the therapy was well-tolerated, leading to no death or side-effect of the subjects.

**MicroPET/CT imaging for therapy monitoring.** B16F10 xenograft mice were treated with LY2409881 or DMSO and imaged serially. Baseline VCAM-1 expression (before LY2409881 treatment) was determined using microPET/CT when the tumor size reached 50 mm$^3$, then the mice were imaged 1, 2, and 3 weeks after initial treatment just before subsequent weekly dose. When the tumor size achieved 50 mm$^3$,

clear tumor uptake was seen (Figure 8A, week 0). Tumors in both groups continued to grow, but the tumor growth of controls was faster than that of the mice treated with LY2409881. The tumor uptake of our probe showed a significant reduction at week 1 for the LY2409881 treatment group compared with the uptake of baseline (week 0) and DMSO control group (week 0 and 1). This was also verified by the tumor biodistribution study (Figure 8C), which showed tumor uptake decreased from 5.02 ± 0.25% ID/g (week 0) to 3.68 ± 0.27% ID/g (week 1) ($p < 0.05$). On the contrary, a slight increase in uptake (5.15 ± 0.14% ID/g) was observed in the control group at week 1. The tumor uptake in the treated group returned to the pre-therapy level at week 2 and week 3 (Figure 8A), and showed no obvious difference to the control group (Figure 8A and 8C) from week 2 forward. Western blot (Figure 8B) showed VCAM-1 expression at different treatment duration times (0, 1, 2 and 3 weeks, $n$=5 per group). The change trends of VCAM-1 expression level were consistent with the tumor uptake in both treatment and control groups, which suggests the specific binding of $^{68}$Ga-NOTA-VCAM-1$_{scFv}$ to VCAM-1 and microPET/CT imaging of $^{68}$Ga-NOTA-VCAM-1$_{scFv}$ at or before one week can be a predictor of tumor response to LY2409881 treatment.

## DISCUSSION

Some previous studies[11,12,14–17] including one by our laboratory[13] have demonstrated the overexpression and important role of VCAM-1 in atherosclerosis, which recommended it to atherosclerosis molecular imaging. Nowadays, the molecular mechanisms of VCAM-1 overexpression in tumorigenicity and metastasis are drawing interest,[2,4] and VCAM-1 is a potential target for diagnosis and treatment of tumors.[6] In the present study, we first demonstrated that IKK2 inhibitor LY2409881 could influence VCAM-1 overexpression cell proliferation and tumor growth *in vitro* and *in vivo*, indicating LY2409881 has a potential role in the inhibition of VCAM-1 expression and cancer progression. More importantly, we synthesized $^{68}$Ga-NOTA-VCAM-1$_{scFv}$, a VCAM-1 targeted probe, and successfully used it for tumor PET/CT imaging to visualize VCAM-1 expression and monitor LY2409881 therapy. This is the first report of revealing the relation of IKK2 inhibitor LY2409881 and VCAM-1 expression, and successfully monitoring IKK2 inhibitor therapy with microPET/CT using radionuclide labeled scFv of VCAM-1 as a tracer.

Refined disease classification is needed for physicians to find targeted treatment options for personalized medicine,[20] and it is vital to select VCAM-1 positive patients before therapy. Molecular imaging has the superiority of detecting and quantifying VCAM-1 expression levels in tumors as a whole-body imaging modality, especially the PET/CT scanning.[21] Gallium is an easily available diagnostic radionuclide with ideal radioactive decay time for PET and is becoming more and more popular as a tracer in synthesizing clinical radiopharmaceuticals.[22] In our study, the $^{68}$Ga-NOTA-VCAM-1$_{scFv}$ was radiosynthesized at high yield in moderate situation, which were consistent with previously published yields of 99% and 90% ± 5%.[23,24] In comparison with the large molecular weight of intact monoclonal antibodies, scFv has the

superiority of lower concentration in liver, rapid blood clearance, and strong penetration into tumor tissue,[13,25] which conforms to the physical half-life of $^{68}$Ga (67.6 min) as radionuclide imaging probes.

From our results, $^{68}$Ga-NOTA-VCAM-1$_{scFv}$ has a high stability and optimistic affinity to VCAM-1 in microPET imaging. LY2409881, as an inhibition reagent, partially blocked the binding of $^{68}$Ga-NOTA-VCAM-1$_{scFv}$ to B16F10 cells and down-regulated tumor uptake *in vivo*, also confirming the binding affinities and specificities of $^{68}$Ga-NOTA-VCAM-1$_{scFv}$ to VCAM-1. $^{68}$Ga-NOTA-VCAM-1$_{scFv}$ could be swept quickly from the blood, and the high radioactivity in kidneys indicated them as the main excretory organs. Similarly, scFv$^{42}{}_{18}$, labeled with $^{68}$Ga, had the same excretion pathway and mainly accumulated in kidneys (42.67–39.06% ID/g, 1–3 h).[26] This could be largely attributed to the small molecular size of scFv (28 KDa). It should be noticed that the bone uptake is a little bit high and constant, which is probably because of free $^{68}$Ga. Free $^{68}$Ga can be absorbed by the bone. The mechanism is that gallium can combine with hydroxyapatite, which is in the bone tissue, and quickly bind to the center of osteogenesis to enter the metabolically active cells. In our study, the uptake in B16F10 tumor was 6.11 ± 0.55, 5.71 ± 0.47, and 5.17 ± 0.68% ID/g at 0.5, 1, and 3 h post-injection, respectively, which is higher than that of VCAM-1-$^{111}$In peptide distribution in omentum of SKOV3ip1 cells (about 2% ID/g).[18] Liu et al.[27] reported $^{68}$Ga-labeled gelatinase inhibitor cyclic peptide also had a lower uptake in tumors (0.88 ± 0.08% ID/g, 60 min). The difference was mainly due to a higher binding affinity of scFv than peptides.

To meet the need for individualized and molecular approach to precision medicine,[28] we focused on the down-regulation of VCAM-1 and selected melanoma as a therapy model. As an extremely malignant tumor, melanoma responds poorly to conventional chemotherapeutics and radiation owing to aggressive tumor progression and hematogenous metastases in the early phase.[29] The persistent activation of NF-κB, mainly due to IKKs, could produce a series of chemokines, which lead to angiogenesis and tumorigenesis.[30] Compared with temozolomide, a common chemotherapy drug, LY2409881 resulted in a stronger inhibition of the viability and proliferation of B16F10 cells *in vitro* from our results. And *in vivo*, our results strongly prove that LY2409881 can repress VCAM-1 expression, inhibit tumor growth and prolong median survival time in melanoma. Moreover, the LY2409881 treatment is well tolerated, resulting in no hematologic effects or decrease in hepatic or renal function during the therapy, suggesting the safety and efficacy of LY2409881. Accordingly, it is reasonable for us to assume that LY2409881 may be an alternative therapeutic approach for VCAM-positive tumor treatment. In contrast, HA15 and BMS-345541 (anticancer drugs) also applied in melanoma have been found to be much more efficacious, with tumor size < 1000 mm$^3$ at 3 weeks.[30,31] Despite weaker inhibition as a limitation, LY2409881 may still be useful in multidrug therapy, and has been found to act in synergy with other anticancer drugs.[9]

Targeted therapy is mounting in popularity in tumor treatment and the accurate monitoring of therapy efficacy has been the key challenges in clinical application.[32,33] With LY2409881 therapy, the expression of

VCAM-1 reduced initially and returned to pretreatment level, which was identified by western blot and biodistribution, and the increase was mainly due to the rapid growth of the tumor. The probe uptakes in the tumor markedly decreased at 1 week, which were consistent with VCAM-1 expression, confirming that LY2409881 had effective and early intervention on VCAM-1, and $^{68}$Ga-NOTA-VCAM-1$_{scFv}$ could be an inchoate predictor of tumor response to LY2409881 intervention. Apart from early diagnosis of the tumor, $^{68}$Ga-NOTA-VCAM-1$_{scFv}$ helped to visually monitor the changes in VCAM-1 expression of VCAM-1 positive xenografts after LY2409881 therapy in an early stage.

In the VCAM-1 inhibition assays, we used $^{68}$Ga-NOTA-VCAM-1$_{scFv}$ and anti-VCAM-1 antibody (which used in western blot) to identify the effect of LY2409881 treatment. The principles for both $^{68}$Ga-NOTA-VCAM-1$_{scFv}$ detection and western blot are based on the antigen-antibody reaction. The detection of VCAM-1 expression by $^{68}$Ga-NOTA-VCAM-1$_{scFv}$ is mainly based on the binding of radioactivity molecules to the antigen. After the immune response, the radioactivity signals of radioactivity molecules are measured to detect the corresponding antigens quantitatively. The method is characterized by high sensitivity and simple operation. Based on the antigen-antibody reaction, western blot is the most widely used method in biological experiments. It uses the chemiluminescence method for quantitative testing. Despite high specificity, its operation steps are complicated, and it needs to get specimen which is invasive and hard to repeat in the living body. The results of these two methods are consistent, indicating that $^{68}$Ga-NOTA-VCAM-1$_{scFv}$ has the potential to be used to detect VCAM-1 noninvasively and repeatedly *in vivo*.

There are some limitations to our study. First, further studies and convincible evidence are required to explore the mechanistic role of LY2409881 in VCAM-1. Second, our study took only the melanoma tumor models as the research object. However, not only melanoma tumor, but also a series of tumors which express VCAM-1, including kidney cancer, breast cancer, ovarian cancer, could benefit from this study.[2,5] Likewise, $^{68}$Ga-NOTA-VCAM-1$_{scFv}$ could theoretically bind to these tumors. We speculate that the probe can be applied in the diagnosis, classification and monitoring treatment of tumors, display maximum benefit, and provide the best opportunity of achieving good health for patients.

**Conclusion**

In conclusion, LY2409881, an IKKβ inhibitor, could suppress the tumor by VCAM-1 inhibition. $^{68}$Ga-NOTA-VCAM-1$_{scFv}$, an easily synthesized tracer, has a potential clinical application in the visual monitoring of LY2409881 tumor curative effect.

**Acknowledgments**

This work was funded by the National Natural Science Foundation of China (No. 81271623 and No.

81630049), and Clinical Research Physician Program of Tongji Medical College, Huazhong University of Science and Technology (5001530008).

**Supporting Information**

VCAM-1 expression confirmed by immunofluorescence, western blot and immunohistochemistry

**References**

(1) Chakraborty, S.; Hu, S. Y.; Wu, S. H.; Karmenyan, A.; Chiou, A. The interaction affinity between vascular cell adhesion molecule-1 (VCAM-1) and very late antigen-4 (VLA-4) analyzed by quantitative FRET. *PloS One* **2015**, *10* (3), e0121399.

(2) Schlesinger, M.; Bendas, G. Vascular cell adhesion molecule-1 (VCAM-1)--an increasing insight into its role in tumorigenicity and metastasis. *Int. J. Cancer* **2015**, *136* (11), 2504-14.

(3) Lin, K. Y.; Lu, D.; Hung, C. F.; Peng, S.; Huang, L.; Jie, C.; Murillo, F.; Rowley, J.; Tsai, Y. C.; He, L.; Kim, D. J.; Jaffee, E.; Pardoll, D.; Wu, T. C. Ectopic expression of vascular cell adhesion molecule-1 as a new mechanism for tumor immune evasion. *Cancer Res.* **2007**, *67* (4), 1832-41.

(4) Lu, X.; Mu, E.; Wei, Y.; Riethdorf, S.; Yang, Q.; Yuan, M.; Yan J.; Hua, Y.; Tiede, B. J.; Lu, X.; Haffty, B. G.; Pantel, K.; Massagué, J.; Kang, Y. VCAM-1 promotes osteolytic expansion of indolent bone micrometastasis of breast cancer by engaging α4β1-positive osteoclast progenitors. *Cancer Cell* **2011**, *20* (6), 701-14.

(5) Huang, J.; Zhang, J.; Li, H.; Lu, Z.; Shan, W.; Mercado-Uribe, I.; Liu, J. VCAM1 expression correlated with tumorigenesis and poor prognosis in high grade serous ovarian cancer. *Am. J. Transl. Res.* **2013**, *5* (3), 336-46.

(6) Chen, Q.; Massagué, J. Molecular pathways: VCAM-1 as a potential therapeutic target in metastasis. *Clin. Cancer. Res.* **2012**, *18* (20), 5520-5.

(7) Peduto, L. ADAM9 as a potential target molecule in cancer. *Curr. Pharm. Des.* **2009**, *15* (20), 2282-7.

(8) Rajmani, R. S.; Gandham, R. K.; Gupta, S. K.; Sahoo, A. P.; Singh, P. K.; Saxena, S.; Kumar, R.; Chaturvedi, U.; Tiwari, A. K. Administration of IκB-kinase inhibitor PS1145 enhances apoptosis in DMBA-induced tumor in male Wistar rats. *Cell Biol. Int.* **2015**, *39* (11), 1317-28.

(9) Deng, C.; Lipstein, M.; Rodriguez, R.; Serrano, X. O.; Mclntosh, C.; Tsai, W. Y.; Wasmuth, A. S.; Jaken, S.; O'Connor, O. A. The novel IKK2 inhibitor LY2409881 potently synergizes with histone deacetylase inhibitors in preclinical models of lymphoma through the downregulation of NF-κB. *Clin. Cancer Res.* **2014**, *21* (1), 134-45.

(10) Li, C.; Wen, B.; Wang, L.; Feng, H.; Xia, X.; Ding, Z.; Gao, B.; Zhang, Y.; Lan, X. $^{99}$mTc-labeled single-domain antibody EG2 in targeting epidermal growth factor receptor: an in-vitro and mouse model in-vivo study. *Nucl. Med. Commun.* **2015,** *39* (5), 452-60.

(11) Kaufmann, B. A.; Carr, C. L.; Belcik, J. T.; Xie, A.; Yue, Q.; Chadderdon, S.; Caplan, E. S.; Khangura, J.; Bullens, S.; Bunting, S.; Lindner, J. R. Molecular imaging of the initial inflammatory response in atherosclerosis: implications for early detection of disease. *Arterioscler. Thromb. Vasc. Biol.* **2010**; *30* (1), 54-9.

(12) Belliere, J.; Lizarrondo, S. M. D.; Choudhury, R. P.; Quenault, A.; Béhot, A.L.; Delage, C.; Chauveau, D.; Schanstra, J. P.; Bascands, J. L.; Vivien, D.; Gauberti, M. Unmasking Silent Endothelial Activation in the Cardiovascular System Using Molecular Magnetic Resonance Imaging. *Theranostics* **2015**, *5* (11), 1187-202.

(13) Liu, C.; Zhang, X.; Song, Y.; Wang, Y.; Zhang, F.; Zhang, Y.; Zhang, Y.; Lan, X. SPECT and fluorescence imaging of vulnerable atherosclerotic plaque with a vascular cell adhesion molecule 1 single-chain antibody fragment. *Atherosclerosis* **2016**, *254*, 263-270.

(14) Bala, G.; Blykers, A.; Xavier, C.; Descamps, B.; Broisat, A.; Ghezzi, C.; Fagret, D.; Camp, G. V.; Caveliers, V.; Vanhove, C.; Lahoutte, T.; Droogmans, S.; Cosyns, B.; Devoogdt, N.; Hernot, S. Targeting of vascular cell adhesion molecule-1 by 18F-labelled nanobodies for PET/CT imaging of inflamed atherosclerotic plaques. *Eur. Heart J. Cardiovasc. Imaging* **2016**, *17* (9), 1001-8.

(15) Broisat, A.; Hernot, S.; Toczek, J.; De, V. J.; Riou, L. M.; Martin, S.; Ahmadi, M.; Thielens, N.; Wernery, U.; Caveliers, V.; Muyldermans, S.; Lahoutte, T.; Fagret, D.; Ghezzi, C.; Devoogdt, N. Nanobodies targeting mouse/human VCAM1 for the nuclear imaging of atherosclerotic lesions. *Circ. Res.* **2012**, *110* (7), 927-37.

(16) Nahrendorf, M.; Keliher, E.; Panizzi, P.; Zhang, H.; Hembrador, S.; Figueiredo, J. L.; Aikawa, E.; Kelly, K.; Libby, P.; Weissleder, R. 18F-4V for PET-CT imaging of VCAM-1 expression in inflammatory atherosclerosis. *JACC. Cardiovasc. Imaging* **2009**, 2 (10), 1213-22.

(17) Dimastromatteo, J.; Broisat, A.; Perret, P.; Ahmadi, M.; Boturyn, D.; Dumy, P.; Fagret, D.; Riou, L. M.; Ghezzi, C. In vivo molecular imaging of atherosclerotic lesions in ApoE-/- mice using VCAM-1-specific, 99mTc-labeled peptidic sequences. *J. Nucl. Med.* **2013**, *54* (8), 1442-9.

(18) Scalici, J. M.; Thomas, S.; Harrer, C.; Raines, T. A.; Curran, J.; Atkins, K. A.; Conaway, M. R.; Duska, L.; Kelly, K. A.; Slack-Davis, J. K. Imaging VCAM-1 as an indicator of treatment efficacy in metastatic ovarian cancer. *J. Nucl. Med.* **2013**, *54* (11), 1883-9.

(19) Hammers, C. M.; Stanley, J. R. Antibody Phage Display: Technique and Applications. *J. Invest. Dermatol.* **2014**, *134* (2), e17.

(20) Jameson, J. L.; Longo, D. L. Precision Medicine--personalized, problematic, and promising. *N. Engl. J. Med.* **2015**, *372* (23), 2229-34.

(21) Kenny, L. M.; Aboagye, E. O. Clinical translation of molecular imaging agents used in PET studies of cancer. *Adv. Cancer. Res.* **2014**, *124*, 329-74.

(22) Velikyan, I. Prospective of $^{68}$Ga-radiopharmaceutical development. *Theranostics* **2013**, *4* (1), 47-80.

(23) Xu, B.; Li, X.; Yin, J.; Liang, C.; Liu, L.; Qiu, Z.; Yao, L.; Nie, Y.; Wang, J.; Wu, K. Evaluation of 68Ga-labeled MG7 antibody: a targeted probe for PET/CT imaging of gastric cancer. *Sci. Rep.* **2015**, *5*, 8626.

(24) Israel, I.; Richter, D.; Stritzker, J.; Ooschot, M. V.; Donat, U.; Buck, A. K.; Samnick, S. PET imaging with [$^{68}$Ga]NOTA-RGD for prostate cancer: a comparative study with [$^{18}$F]fluorodeoxyglucose and [$^{18}$F]fluoroethylcholine. *Curr. Cancer Drug Targets* **2014**; *14* (4), 371-9.

(25) Han, D.; Wu, J.; Han, Y.; Wei, M.; Han, S.; Lin, R.; Sun, Z.; Yang, F.; Jiao, D.; Xie, P.; Zhang, L.; Yang, A. G.; Zhao, A.; Wen, W.; Qin, W. A novel anti-PSMA human scFv has the potential to be used as a diagnostic tool in prostate cancer. *Oncotarget* **2016**, *7* (37), 59471-81.

(26) Eder, M.; Knackmuss, S.; Le, G. F.; Reusch, U.; Rybin, V.; Little, M.; Haberkorn, U.; Mier, W.; Eisenhut, M. 68Ga-labelled recombinant antibody variants for immuno-PET imaging of solid tumours. *Eur. J. Nucl. Med. Mol. Imaging* **2010**, *37* (7), 1397-407.

(27) Liu, Q.; Pan, D.; Cheng, C.; Zhang, A.; Ma, C.; Wang, L.; Zhang, D.; Liu, H.; Jiang, H.; Wang, T.; Xu, Y.; Yang, R.; Chen, F.; Yang, M.; Zuo, C. Targeting of MMP2 activity in malignant tumors with a 68Ga-labeled gelatinase inhibitor cyclic peptide. *Nucl. Med. Biol.* **2015**, *42* (12), 939-44.

(28) Collins, F. S.; Varmus, H. A new initiative on precision medicine. *N. Engl. J. Med.* **2015**, *372* (9), 793-5.

(29) Feng, H.; Xia, X.; Li, C.; Song, Y.; Qin, C.; Liu, Q.; Zhang, Y.; Lan, X. Imaging malignant melanoma with (18)F-5-FPN. *Eur. J. Nucl. Med. Mol. Imaging* **2016**, *43* (1), 113-22.

(30) Yang, J.; Amiri, K. I.; Burke, J. R.; Schmid, J. A.; Richmond, A. BMS-345541 targets inhibitor of kappaB kinase and induces apoptosis in melanoma: involvement of nuclear factor kappaB and mitochondria pathways. *Clin. Cancer Res.* **2006**, *12* (3 Pt 1), 950-60.

(31) Cerezo, M.; Lehraiki, A.; Millet, A.; Rouaud, F.; Plaisant, M.; Jaune, E.; Botton, T.; Ronco, C.; Abbe, P.; Amdouni, H.; Passeron, T.; Hofman, V.; Mograbi, B.; Dabert-Gay, A. S.; Debayle, D.; Alcor, D.; Rabhi, N.; Annicotte, J. S.; Héliot, L.; Gonzalez-Pisfil, M.; Robert, C.; Moréra, S.; Vigouroux, A.; Gual, P.; Ali, M. M. U.; Bertolotto, C.; Hofman, P.; Ballotti, R.; Benhida, R.; Rocchi, S. Compounds Triggering ER Stress Exert Anti-Melanoma Effects and Overcome BRAF Inhibitor Resistance. *Cancer Cell* **2016**, *29* (6), 805-19.

(32) Teng, F. F.; Meng, X.; Sun, X. D.; Yu, J. M. New strategy for monitoring targeted therapy: molecular imaging. *Int. J. Nanomedicine* **2013**, *8*, 3703-13.

(33) Bilt, A. R. V. D.; Terwisscha, V. S. A. G.; Timmer-Bosscha, H.; Schröder, C. P.; Pot. L.; Kosterink, J. G.; Zee, A. G. V. D., Lub-de, H. M. N.; Jong, S. D.; Vries, E. G. D.; Reyners, A. K. Measurement of tumor VEGF-A levels with 89Zr-bevacizumab PET as an early biomarker for the antiangiogenic effect of everolimus treatment in an ovarian cancer xenograft model. *Clin. Cancer Res.* **2012**, *18* (22), 6306-14.

**Figure Legends**

**Figure 1.** The mechanism of monitoring vascular cell adhesion molecule 1 (VCAM-1) changes with $^{68}$Ga-NOTA-VCAM-1$_{scFv}$ after LY2309881 therapy. LY2409881 specifically inhibits the expression of IKK2, which inhibits the NF-κB expression and then reduces VCAM-1 expression. The chelator NOTA was used to label the single chain variable fragment (scFv) of VCAM-1 with $^{68}$Ga.

**Figure 2.** Flow chart of the treatment groups.

**Figure 3.** Cell Immunofluorescence of VCAM-1 in B16F10 and A375m cells (A). B16F10 (upper row) and A375m (lower row) cells were incubated with VCAM-1 antibody (red) and nuclei were stained with DAPI. Representative images are displayed at the same scale (×600). Western blot was used to examine the expression levels of VCAM-1 protein in B16F10 and A375m cells, and GAPDH used as the internal control (B). The semi-quantitative analysis was accomplished using the integrated optical density ratio of VCAM-1 to GADPH (C). $*p < 0.05$. All data are the means ± SD in triplicate.

**Figure 4.** Representative microPET/CT images of $^{68}$Ga-NOTA-VCAM-1$_{scFv}$ in tumor xenografts. The images of B16F10 tumor-bearing mice were acquired at 0.5, 1, and 3 h after injection (A), and A375m tumor-bearing mice at 3 h (B). The A375m tumor is indicated by a red arrow. In autoradiography, much higher tracer uptake in B16F10 tumor was seen than that in A375m tumor (C, D). Activity in kidney and liver was similar for the two tumors. The expression levels of VCAM-1 in tumors were also confirmed by immunohistochemistry (E, ×400).

**Figure 5.** Biodistribution of $^{68}$Ga-NOTA-VCAM-1$_{scFv}$ in mouse xenograft tumors. A and B represent B16F10 and A375m tumor bearing models, respectively. C shows the tumor uptake of the tracer in different time points after injection of the tracer in B16F10 and A375m tumor models. D and E show the tumor-to-muscle ratio (T/M) and tumor-to-blood ratio (T/B) of B16F10 and A375m tumor-bearing mice at 0.5, 1, and 3 h. $*p < 0.01$, $**p < 0.001$ and $***p < 0.0001$. The data are expressed as the mean ± SD ($n$=5).

**Figure 6.** Western blot results of VCAM-1 protein expression with LY2409881 treatment in B16F10 cells with GAPDH as an internal control (A). The semi-quantitative analysis was calculated using integrated optical density ratio of VCAM-1 to GADPH (B). The LY2409881 influence on B16F10 cell uptake was performed at various concentrations (0, 1, 2, 5, 10 and 20 μM) for 12 h, followed by incubation with $^{68}$Ga-NOTA-VCAM-1$_{scFv}$ (2 nM) at 37°C for 120 min (C). The cell viability of B16F10 (D) determined by CCK8 was performed at designated time intervals (24, 48 and 72 h) after LY2409881 (1, 2, 5, 10, 20, 30 and 40 μM) treatment. The pharmacologic activity of temozolomide (100, 200, 400, 600 and 800 μM) in

B16F10 cells as a drug control is shown in E. *$p < 0.01$ and **$p < 0.001$. LY represents LY2409881. All data are the means ± SD in triplicate.

**Figure 7.** The *in vivo* inhibition of LY2409881 in B16F10 tumor models. Tumor volume and weight were measured every two days for a total of 21 days since the tumor volume reached 50 $mm^3$. Tumor volume curves and weight curves of LY2409881 treatment and DMSO control are shown in A and B ($n$=10 per group). The mice began to die on day 22 and the surviving percentage in the treated mice relative to the untreated mice was expressed as a function of the time evolution (C, $n$=10 per group). H&E staining of liver, kidney and spleen at different therapy duration are shown in D (×200, $n$=5 per group). *$p < 0.05$, **$p < 0.01$ and ***$p < 0.001$. LY represents LY2409881 and D represents DMSO. All data are expressed as the means ± SD.

**Figure 8.** A series of sequential tomographic images of the same B16F10 tumor bearing mice at 0, 1, 2 and 3 weeks after treatment with LY2409881 (100 mg/kg, twice weekly) or DMSO-control (A, upper row is coronal plane, and lower row is transverse plane). Red arrows indicate tumors. The tumors of the baseline, treatment and control mice (0, 1, 2 and 3 weeks, $n$=5 per group) were analyzed VCAM-1 expression with western blot (B). Comparison of tumor biodistribution in two groups before and after LY2409881 or DMSO treatment (0, 1, 2 and 3 weeks, $n$=5 per group, C). *$p < 0.01$.

**Tables**

**Table 1.** The routine blood test results of the LY2409881 treatment group and control DMSO treatment group (means ± SD, *n*=5).

| Enrollment | WBC (× $10^9$/L) | RBC (× $10^{12}$/L) | HGB (g/L) | PLT (× $10^9$/L) |
|---|---|---|---|---|
| **Initiation** | 5.37 ± 0.49 | 7.47 ± 0.61 | 115.00 ± 9.54 | 410.00 ± 36.86 |
| **1 W(DMSO)** | 6.93 ± 2.02 | 6.18 ± 1.60 | 80.33 ± 18.66 | 397.70± 138.80 |
| **1 W (LY)** | 5.90 ± 1.24 | 7.19 ± 0.61 | 99.33 ± 10.09 | 392.30 ± 81.54 |
| **2 W (DMSO)** | 8.17 ± 1.16 | 7.39 ± 0.65 | 102.70 ± 8.65 | 369.30 ± 51.40 |
| **2 W (LY)** | 6.67 ± 1.64 | 7.15 ± 0.60 | 100.30± 10.04 | 328.30 ± 37.34 |
| **3 W (DMSO)** | 5.03 ± 0.74 | 8.25 ± 0.50 | 117.00 ± 8.19 | 383.00 ± 86.07 |
| **3 W (LY)** | 6.70 ± 1.23 | 7.62 ± 0.61 | 107.70 ± 9.06 | 414.00 ± 58.48 |

LY represents LY2409881. The results between two groups had no significant difference ($p > 0.05$).

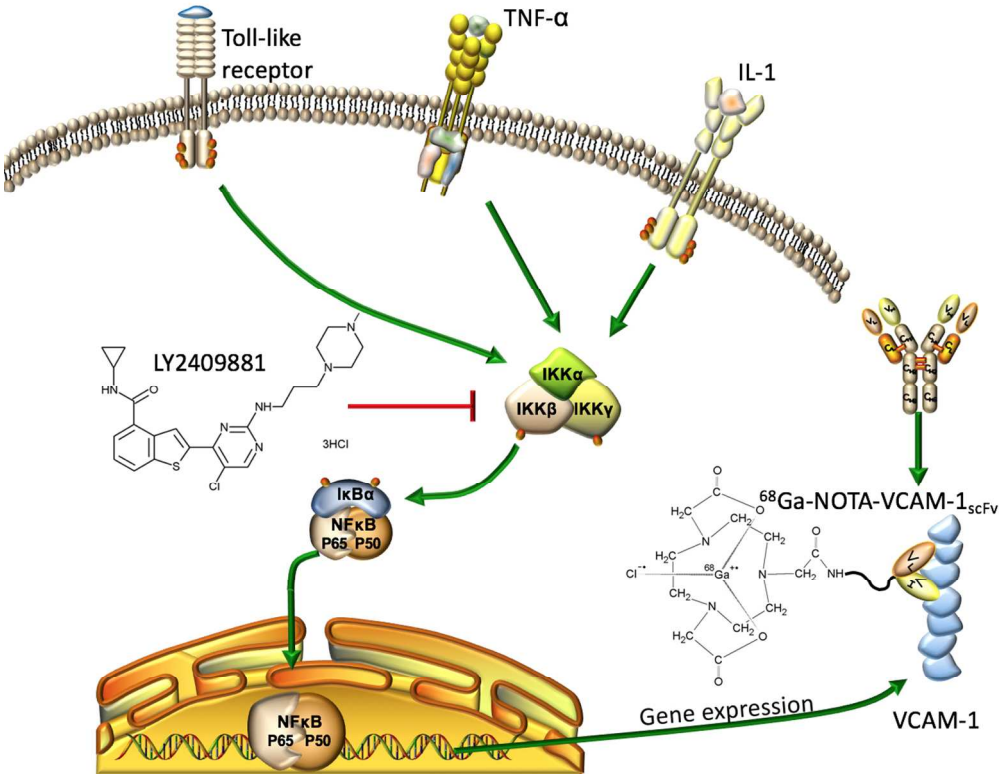


Figure 1. The mechanism of monitoring vascular cell adhesion molecule 1 (VCAM-1) changes with 68Ga-NOTA-VCAM-1scFv after LY2309881 therapy. LY2409881 specifically inhibits the expression of IKK2, which inhibits the NF-κB expression and then reduces VCAM-1 expression. The chelator NOTA was used to label the single chain variable fragment (scFv) of VCAM-1 with 68Ga.

233x180mm (144 x 144 DPI)

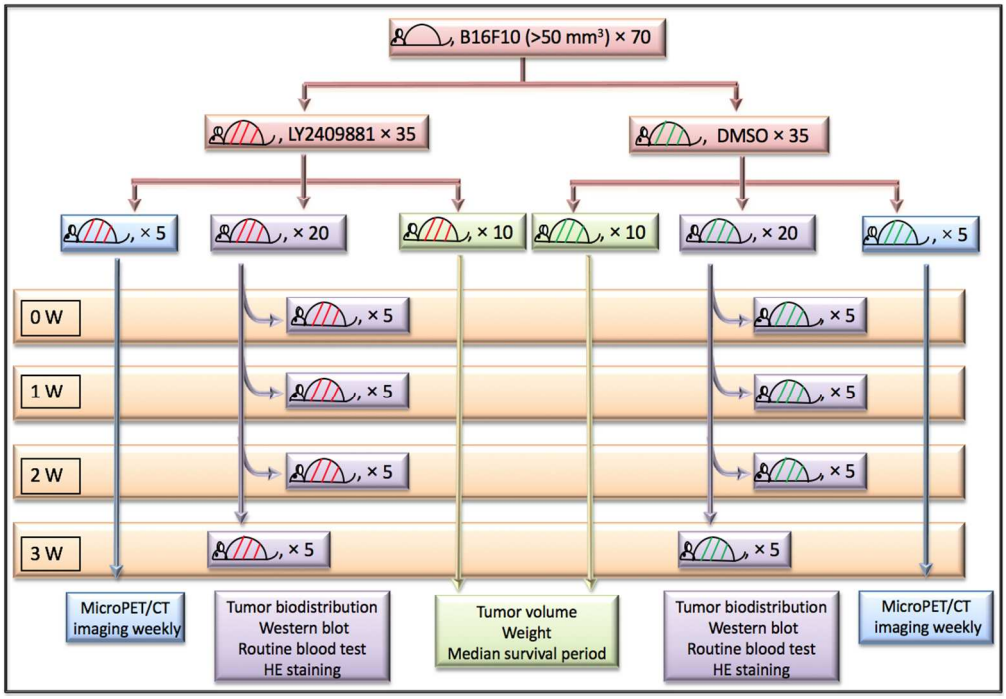


Figure 2. Flow chart of the treatment groups.

223x155mm (144 x 144 DPI)

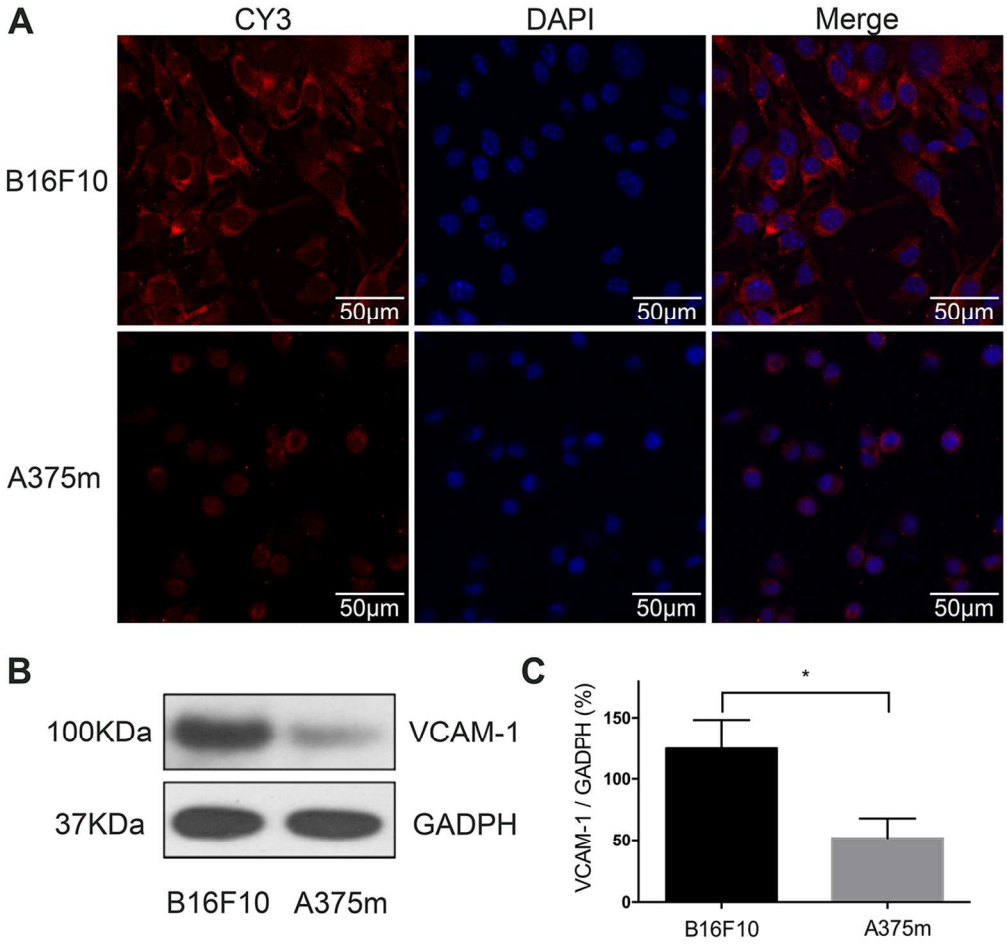


Figure 3. Cell Immunofluorescence of VCAM-1 in B16F10 and A375m cells (A). B16F10 (upper row) and A375m (lower row) cells were incubated with VCAM-1 antibody (red) and nuclei were stained with DAPI. Representative images are displayed at the same scale (×600). Western blot was used to examine the expression levels of VCAM-1 protein in B16F10 and A375m cells, and GAPDH used as the internal control (B). The semi-quantitative analysis was accomplished using the integrated optical density ratio of VCAM-1 to GADPH (C). *$p < 0.05$. All data are the means ± SD in triplicate.

119x112mm (300 x 300 DPI)

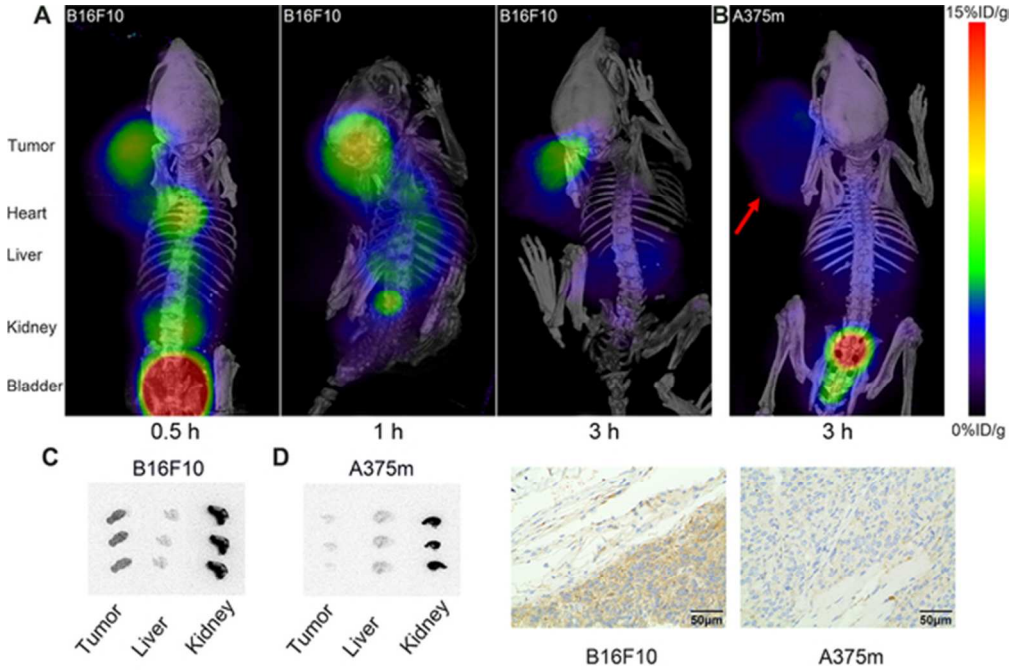


Figure 4. Representative microPET/CT images of 68Ga-NOTA-VCAM-1scFv in tumor xenografts. The images of B16F10 tumor-bearing mice were acquired at 0.5, 1, and 3 h after injection (A), and A375m tumor-bearing mice at 3 h (B). The A375m tumor is indicated by a red arrow. In autoradiography, much higher tracer uptake in B16F10 tumor was seen than that in A375m tumor (C, D). Activity in kidney and liver was similar for the two tumors. The expression levels of VCAM-1 in tumors were also confirmed by immunohistochemistry (E, ×400).

53x35mm (300 x 300 DPI)

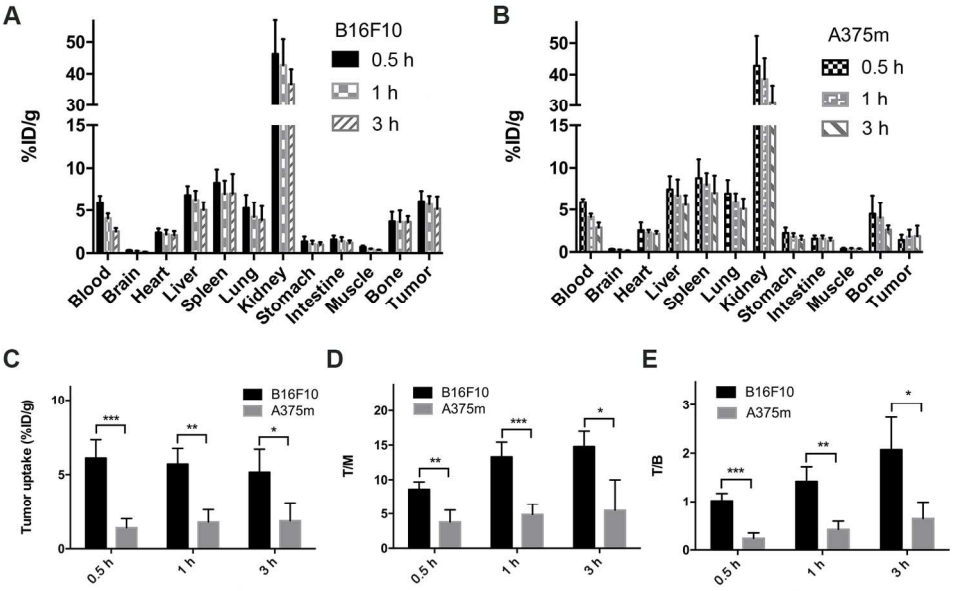


Figure 5. Biodistribution of 68Ga-NOTA-VCAM-1scFv in mouse xenograft tumors. A and B represent B16F10 and A375m tumor bearing models, respectively. C shows the tumor uptake of the tracer in different time points after injection of the tracer in B16F10 and A375m tumor models. D and E show the tumor-to-muscle ratio (T/M) and tumor-to-blood ratio (T/B) of B16F10 and A375m tumor-bearing mice at 0.5, 1, and 3 h. *p < 0.01, **p < 0.001 and ***p < 0.0001. The data are expressed as the mean ± SD (n=5).

165x99mm (300 x 300 DPI)

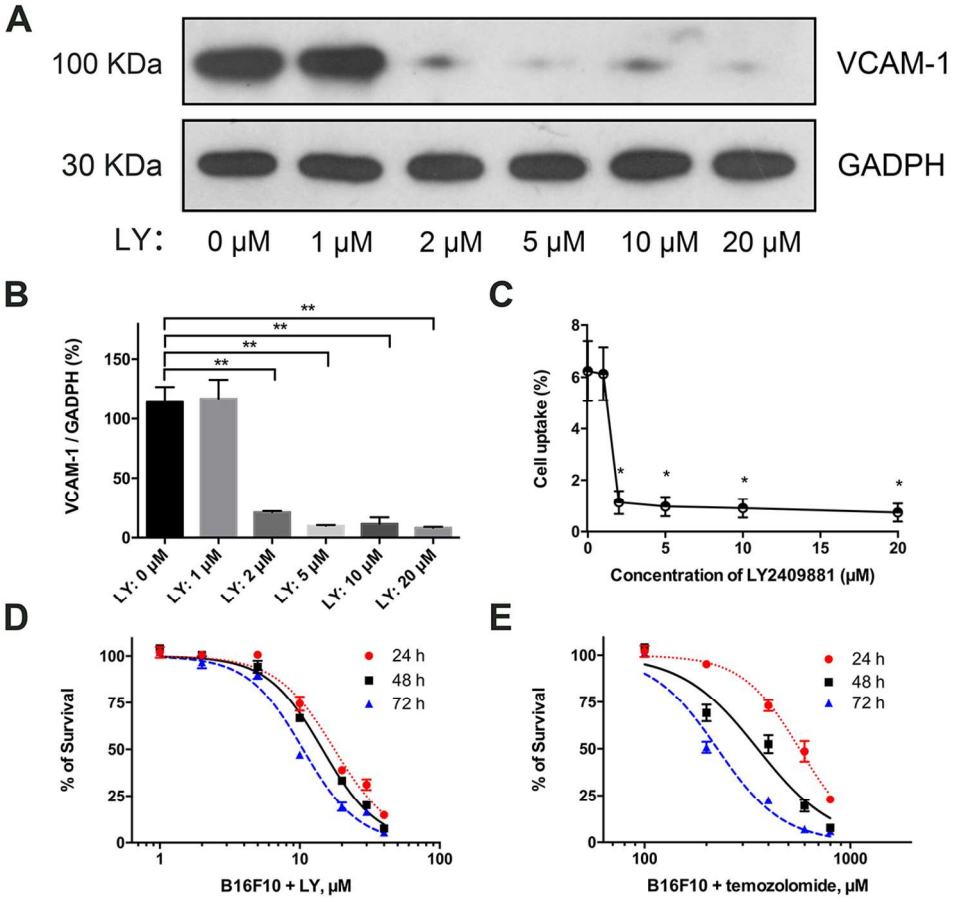


Figure 6. Western blot results of VCAM-1 protein expression with LY2409881 treatment in B16F10 cells with GAPDH as an internal control (A). The semi-quantitative analysis was calculated using integrated optical density ratio of VCAM-1 to GADPH (B). The LY2409881 influence on B16F10 cell uptake was performed at various concentrations (0, 1, 2, 5, 10 and 20 μM) for 12 h, followed by incubation with 68Ga-NOTA-VCAM-1scFv (2 nM) at 37°C for 120 min (C). The cell viability of B16F10 (D) determined by CCK8 was performed at designated time intervals (24, 48 and 72 h) after LY2409881 (1, 2, 5, 10, 20, 30 and 40 μM) treatment. The pharmacologic activity of temozolomide (100, 200, 400, 600 and 800 μM) in B16F10 cells as a drug control is shown in E. *p < 0.01 and **p < 0.001. LY represents LY2409881. All data are the means ± SD in triplicate.

115x103mm (300 x 300 DPI)

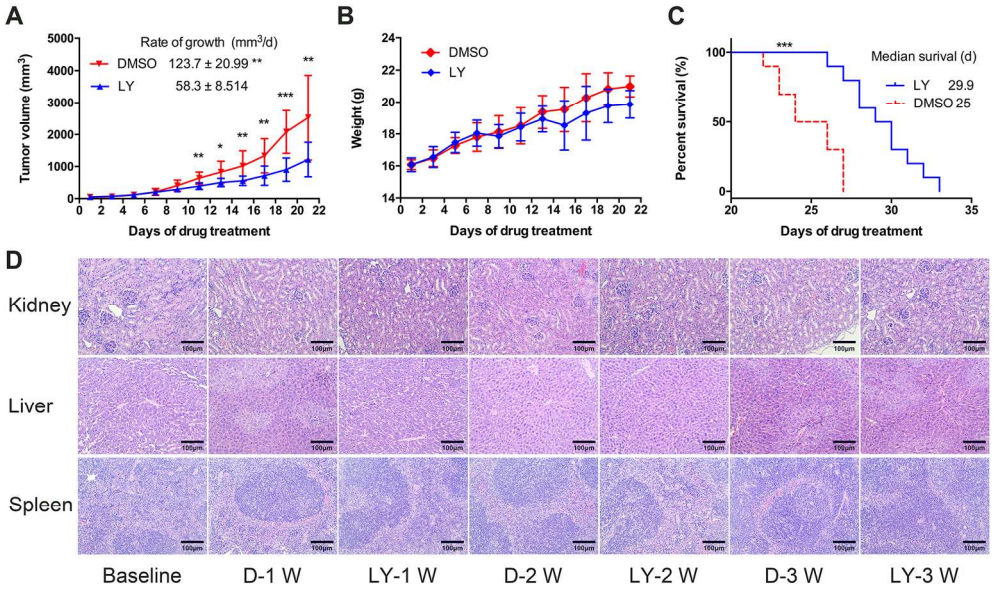


Figure 7. The in vivo inhibition of LY2409881 in B16F10 tumor models. Tumor volume and weight were measured every two days for a total of 21 days since the tumors volume reached 50 mm3. Tumor volume curves and weight curves of LY2409881 treatment and DMSO control are shown in A and B (n=10 per group). The mice began to die at day 22 and the surviving percentage in the treated mice relative to the untreated mice was expressed as a function of the time evolution (C, n=10 per group). H&E staining of liver, kidney and spleen at different therapy duration are shown in D (×200, n=5 per group). *$p < 0.05$, **$p < 0.01$ and ***$p < 0.001$. LY represents LY2409881 and D represents DMSO. All data are expressed as the means ± SD.

170x102mm (300 x 300 DPI)

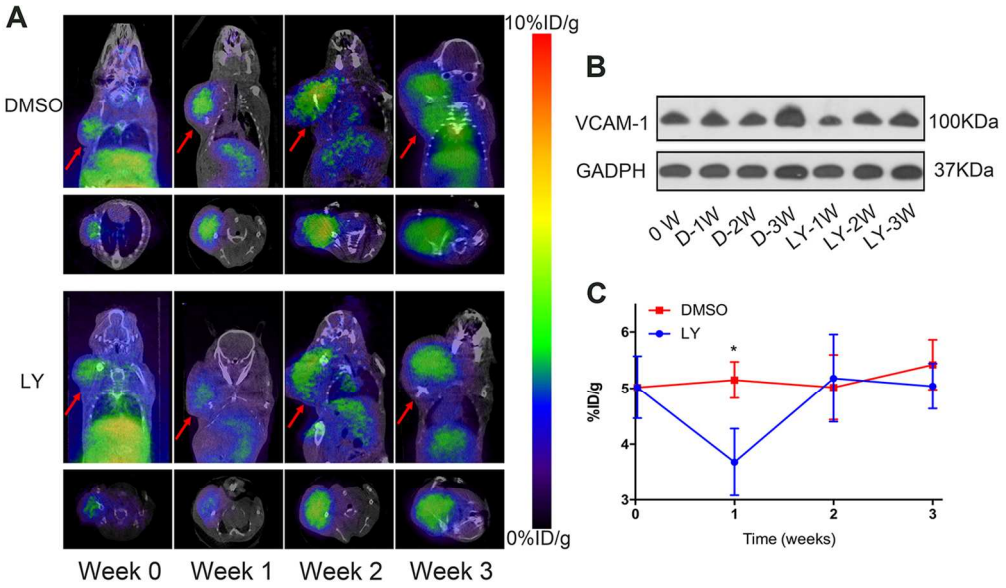


Figure 8. A series of sequential tomographic images of the same B16F10 tumor bearing mice at 0, 1, 2 and 3 weeks after treatment with LY2409881 (100 mg/kg, twice weekly) or DMSO-control (A, upper row is coronal plane, and lower row is transverse plane). Red arrows indicate tumors. The tumors of the baseline, treatment and control mice (0, 1, 2 and 3 weeks, n=5 per group) were analyzed VCAM-1 expression with western blot (B). Comparison of tumor biodistribution in two groups before and after LY2409881 or DMSO treatment (0, 1, 2 and 3 weeks, n=5 per group, C). *p < 0.01.

140x81mm (300 x 300 DPI)